# Exploring the potential of interleaving to delay catastrophic failure in unidirectional composites under tensile loading

Gaël Grail[a,*], Soraia Pimenta[b], Silvestre Pinho[a], Paul Robinson[a]

[a] *The Composites Centre, Department of Aeronautics, South Kensington Campus, Imperial College London, SW7 2AZ, United Kingdom*

[b] *The Composites Centre, Department of Mechanical Engineering, South Kensington Campus, Imperial College London, SW7 2AZ, United Kingdom*

**Abstract**

This work investigates the potential of interleaving to delay catastrophic translaminar failure in unidirectional Carbon Fibre Reinforced Polymers (CFRPs) under tensile load. A Finite Element Model of a damaged Polymer Interleaved Composite (PIC) specimen was built by considering an initial translaminar crack in a CFRP ply, and cohesive zones across the neighbouring interleaves and interleaf/CFRP interfaces. Under tensile load, two competing damage processes (delamination and interleaf yielding/cracking) are predicted, leading to different stress concentrations in the neighbouring CFRP plies for different interleaf geometries and material properties. The probability of unstable through-the-thickness crack propagation is then calculated, considering the strength variability of CFRP plies. Results showed that: (i) a high strength variability in CFRP plies leads to a more stable crack propagation in PICs, which can be achieved by using a low number of fibres in each CFRP ply, and (ii) the geometry and mechanical properties of the PIC can be designed to promote controlled delamination, thereby decreasing the stress concentration at the neighbouring plies. The potential of interleaving to delay catastrophic translaminar failure lies in this last aspect, which permits a larger critical cluster of broken fibres than that of classical UD composites.

*Keywords:* Finite Element Analysis, Stress concentrations, Stress transfer, Probabilistic methods, Interleaved composite

## 1. Introduction

The brittle behaviour of conventional UniDirectional (UD) Carbon Fibre Reinforced Polymers (CFRPs) under tensile load in the fibre direction is widely reported in the literature. However, experiments [1–3] and modelling [4, 5] show that fibre damage in UD composites

*Corresponding author.
*Email address:* g.grail@imperial.ac.uk (Gaël Grail)

accumulates from very low applied loads, until it reaches a cluster size of broken fibres that leads to catastrophic failure. This paper aims to understand whether it is possible to delay final failure in a UD composite by isolating sub-critical clusters of broken fibres through interleaving (*i.e.* incorporating thin thermoplastic polymer films in between the laminae).

Over the last two decades, interleaving has been studied as a method to enhance the interlaminar damage tolerance of continuous CFRPs. This technique can produce a larger damage zone at the crack tip, which has shown improvements to the delamination fracture toughness of UD composites [6, 7], the residual compressive strength after impact [8–10], and the fatigue performance of UD and cross-ply laminates [11, 12].

The potential of interleaving to delay catastrophic failure of continuous CFRPs under longitudinal tensile load has not been investigated in the literature. However, it is clear that the deformation ability of polymeric interleaves reduces stress concentration in the vicinity of a translaminar ply crack (*i.e.* across fibres), which may provide an efficient isolation mechanism between adjacent CFRP plies. Therefore, interleaving appears to be a suitable candidate for delaying catastrophic failure across the plies.

Experiments and modelling show that, in a typical CFRP, the largest cluster of broken fibres that the composite is able to withstand has approximatively 16–32 fibres [1–5]. While conventional plies have certainly a super-critical number of fibres across their thickness, thin plies [13, 14] have 4–9 fibres across the thickness, which suggests that broken sub-critical clusters in a thin-ply interleaved composite can be isolated by a suitable interleaf material.

The present study investigates the potential of interleaving to delay catastrophic failure of UD composites under longitudinal tensile load. The following objectives are addressed: (i) to predict the effect of the main mechanical and geometrical variables in the design of Polymer Interleaved Composites (PICs) on their failure process, and (ii) to understand which mechanisms could lead to a stable translaminar crack propagation. A Finite Element Model (FEM) of a PIC with thin CFRP plies is defined in Section 2, and the model is used in Section 3 to investigate the stress concentrations in the vicinity of a translaminar single ply crack; the stress fields are used to calculate the probability of unstable failure of the composite in Section 4. Section 5 concludes on the potential of PICs to delay catastrophic failure.

## 2. Polymer interleaved composite modelling

### 2.1. Geometry and mesh of the PIC with one fractured ply

A FEM of a damaged UD thin-ply PIC specimen under tensile load is built by considering an initial translaminar crack in a CFRP ply (see Figure 1). In the vicinity of this crack, load is transferred from the broken ply to its neighbours by shear of the interleaf/interface between plies. The model is used to obtain the stress distributions in the neighbouring CFRP plies (Section 3), and their resulting cumulative failure probability (Section 4).

Figure 1 shows the geometry and the structured mesh of the two-dimensional plane-stress PIC FEM, where the UD CFRP plies and interleaf polymer layers are represented explicitly. The model considers 6 homogenized interleaf polymer layers and 7 homogenized UD CFRP plies with fibres aligned along the direction of the load ($x$–axis). Due to the symmetry, only one quarter of the lay-up is modelled explicitly. A translaminar crack is introduced in the central CFRP ply at $x = 0$, using symmetry and boundary conditions represented in Figure 1.

Convergence studies were performed to verify that the mesh and the model's length ($L$) led to converged results. The element height $h$ in Interleaf 1 is kept constant along the thickness ($y$–axis) and the element width increases linearly along the $x$–axis.

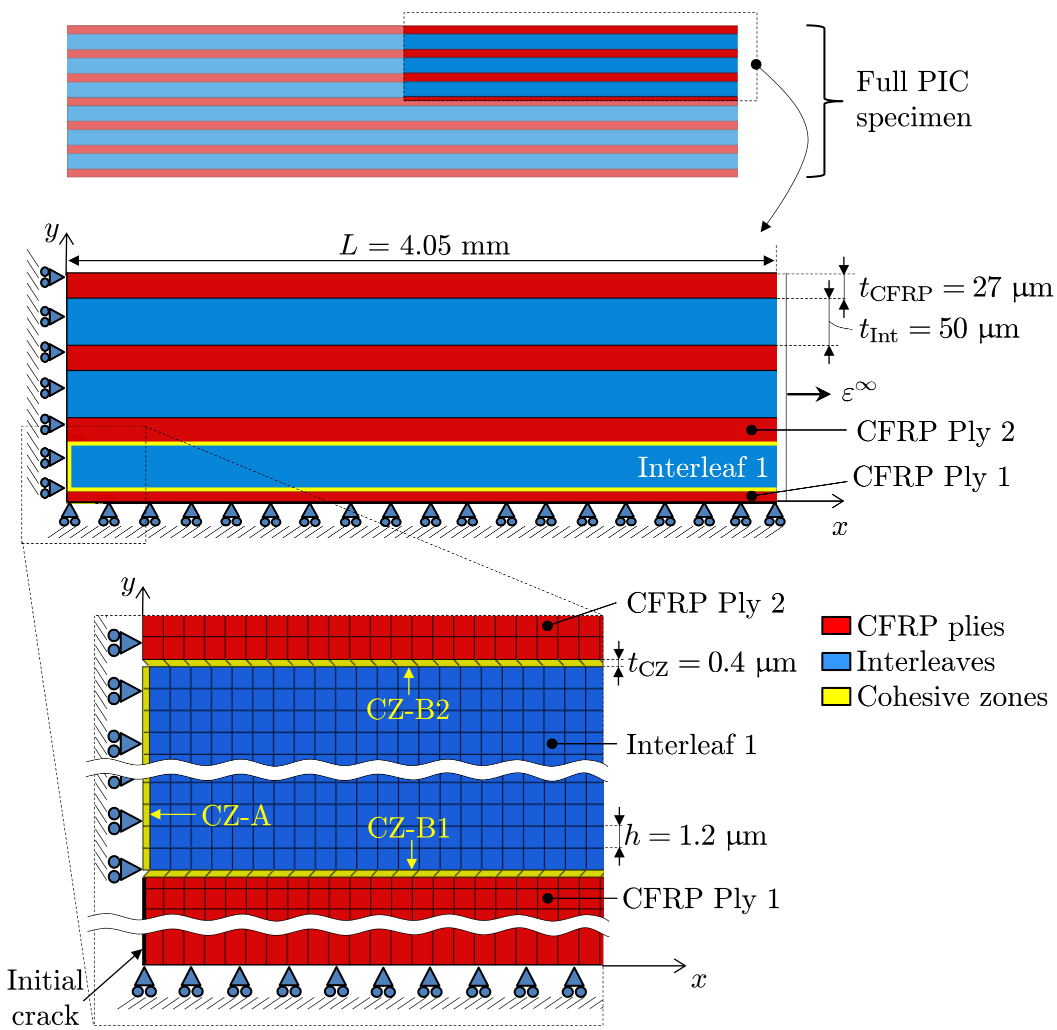


**Figure 1:** Geometry and mesh of the FEM used to analyse the stress field in the vicinity of a broken ply and the resulting failure process (the top two images are not to scale; the bottom image is very zoomed-in, thus the increase of the element width along the $x$–axis is too small to be seen

).

### 2.2. Cohesive zones

#### 2.2.1. Concept of the approach

Three cohesive zones (CZs) were introduced in the FEM: CZ–A in the through-the-thickness direction of Interleaf 1 at the crack plane ($x = 0$), CZ–B1 and CZ–B2 at interfaces between Interleaf 1 and CFRP Ply 1 and 2 respectively, as indicated in Figure 1. This allows the model to capture two different damage processes at the ply level:

A. *transverse interleaf polymer cracking/yielding*, modelled through CZ–A.

B. *delamination at the interleaf/CFRP interfaces*, modelled by CZ–B1 and CZ–B2.

This approach presents several positive characteristics:

- the damage process can consist of multiple crack paths (*i.e.* delamination or interleaf yielding). This approach does not enable migration of delamination, but the latter only occurs for a thick interleaf (thickness over 100 μm) [11, 15, 16].
- both damage initiation and propagation can be controlled through respectively strength and fracture energy parameters of the CZs.
- the properties of the interleaf can be different from those of the CFRP/interleaf interface.

#### 2.2.2. Cohesive laws

Two bilinear traction-separation laws were defined, one for CZ–A and another for both CZ–B1 and CZ–B2. Six parameters per law were required: the penalty stiffness $K$, the maximum traction $T$, and the fracture toughness $G_{\mathrm{c}}$ [17], each for mode I and II. Appendix A details how these parameters were estimated from the known yield stress of the polymer ($\sigma_{\mathrm{YS}}$), the Interfacial Shear Strength (IFSS, $T_{\mathrm{II}}^{\mathrm{B}}$) of the CFRP/interleaf bond, and mode II delamination toughness ($G_{\mathrm{IIc}}^{\mathrm{B}}$) between the interleaf and the CFRP. The estimated parameters are reasonable for this class of materials, and parametric studies are presented in Section 3. Mixed-mode was modelled with a quadratic stress interaction for damage initiation and linear interaction for damage propagation [18].

### 2.3. Mechanical properties

For the sake of simplicity, CFRP and interleaf were assumed elastic, with transverse isotropic and isotropic constitutive behaviours respectively. Non-linearity due to transverse interleaf cracking/yielding near a ply break was modelled with cohesive elements in CZ–A (see Section 2.2), and other sources of non-linearity (such as visco-elasticity/plasticity) were neglected. Chemical interactions between the interleaves and the CFRP plies, leading to different properties between the in-situ and the bulk material, were also neglected. The

CFRP material modelled is a Skyflex USN020A, a thin-ply TR30/K50 (Mitsubishi Rayon/SK Chemicals) carbon-epoxy prepreg with mechanical properties taken from the literature [19], and summarised in Table 1. The reference interleaf polymer is Polyethersulfone (PES), with properties taken from the literature [20–22], and given in Table 2.

### 2.4. Loading and computation

The model was implemented in the finite element code ABAQUS 6.12 [18], and the problem was expressed in an implicit and non-linear geometric formulation (to properly represent large deformations and rotation of elements in the neighbourhood of the initial crack in CFRP Ply 1). The effect of residual thermal stresses has been investigated by other authors [23, 24], but has been neglected in the current study. An uniform displacement was applied at $x = L$ such that the composite specimen was stretched along the fibre direction to a maximum overall strain of 2%. The stress fields in the vicinity of the crack were studied in detail, and a parametric study on the influence of the main mechanical and geometrical variables in the design of PICs was performed using the scripting language Python [25].

### 2.5. Parametric study

The parameters studied were (i) the properties of the CFRP/interleaf interfaces ($T_{\mathrm{II}}^{\mathrm{B}}$, $\sigma_{\mathrm{YS}}$, $G_{\mathrm{IIc}}^{\mathrm{B}}$, and $G_{\mathrm{Ic}}^{\mathrm{A}}$), and (ii) the properties of the interleaf ($E_{\mathrm{Int}}$ and $t_{\mathrm{Int}}$).

The CFRP/interleaf IFSS plays an important role in the failure process. Three values of $T_{\mathrm{II}}^{\mathrm{B}}$ were considered: half the reference value, the reference value (see Table 2), and twice

**Table 1:** Mechanical properties of TR30/K50 CFRP (Skyflex USN020A). Longitudinal and transverse directions are indicated respectively by "l" and "t" in subscript. $E$ and $G$ are the tensile and shear elastic moduli respectively, $\nu$ is the Poisson's ratio, and $V^{\mathrm{f}}$ is the CFRP fibre volume fraction.

| $E_{\mathrm{l}}$ (GPa) | $E_{\mathrm{t}}$ (GPa) | $G_{\mathrm{lt}}$ (GPa) | $\nu_{\mathrm{lt}}$ (-) | $V^{\mathrm{f}}$ (%) |
|---|---|---|---|---|
| 101.7 [19] | $4.8^{(\star)}$ | $1.9^{(\star)}$ | $0.32^{(\star)}$ | $42.5^{(\dagger)}$ |

$^{(\star)}$ Estimated

$^{(\dagger)}$ Measured on 16 ply UD laminates

**Table 2:** Reference mechanical and geometrical properties of the interleaf and its interface to TR30/K50 CFRP, indicated by "ref" in superscript. Parameters related to the interleaf are indicated by "Int" in subscript. Parameters related to the constitutive laws CZ–A and CZs-B are indicated respectively by "A" and "B" in superscript. $G_{\mathrm{Ic}}^{\mathrm{A,ref}}$ was calculated from Equation A.4, $G_{\mathrm{IIc}}^{\mathrm{B,ref}}$ is obtained from experimental End-Notched-Test results [21, 22] performed on interleaved CFRP composite with interlayer thicknesses of the same order of magnitude as the one considered in this study.

| **Mechanical properties** | | | | | | **Geometry** |
|---|---|---|---|---|---|---|
| $E_{\mathrm{Int}}^{\mathrm{ref}}$ (GPa) | $\nu_{\mathrm{Int}}$ (-) | $\sigma_{\mathrm{YS}}^{\mathrm{ref}}$ (MPa) | $T_{\mathrm{II}}^{\mathrm{B,ref}}$ (MPa) | $G_{\mathrm{Ic}}^{\mathrm{A,ref}}$ (kJ.m$^{-2}$) | $G_{\mathrm{IIc}}^{\mathrm{B,ref}}$ (kJ.m$^{-2}$) | $t_{\mathrm{Int}}^{\mathrm{ref}}$ (μm) |
| 2.45 [20] | 0.31 [20] | 80 [20] | 40 [20] | 0.73 | 1.2 [21, 22] | 50 |

the reference value. For each value of $T_{\mathrm{II}}^{\mathrm{B}}$, each of the other parameters were set at half their reference value, their reference value (see Table 2), and twice their reference value.

### 2.6. Normalised stress distribution

The stress distribution in CFRP Ply 2 ($\bar{\sigma}$) is normalised and calculated along its length ($x$), at each value of applied remote strain $\varepsilon^{\infty}$, as

$$\bar{\sigma}(x, \varepsilon^{\infty}) = \frac{\hat{\sigma}(x, \varepsilon^{\infty})}{\hat{\sigma}(L, \varepsilon^{\infty})}, \tag{1}$$

where $\hat{\sigma}$ is the homogenised stress over the through-the-thickness section of CFRP Ply 2, calculated from the FE results. The use of homogenised stresses simplifies the probabilistic analysis in Section 4, and avoids the complexity introduced by extrapolating stress values to the surface of the ply (where the maximum would occur).

## 3. Analysis of stress fields and interleaf damage in a pre-fractured PIC

### 3.1. Results for the analysis of failure process

Figure 2 presents stress distributions in CFRP Ply 2 for the reference properties and geometry given in Table 2, and for three different applied remote strains. Each subfigure 2a, b and c considers a different value of CFRP/interleaf IFSS ($T_{\mathrm{II}}^{\mathrm{B}}$), used for the constitutive law in CZ–B1 and CZ–B2. A zoom of the deformed specimen in the vicinity of the crack under a remote strain of 2% is shown on the left of each graph in Figure 2.

The zoom presented in Figure 2b shows that, for $T_{\mathrm{II}}^{\mathrm{B}}/T_{\mathrm{II}}^{\mathrm{B,ref}} = 1.0$, there are three competing damage propagation processes: (i) CZ–A failing in mode I, (ii) CZ–B1 failing in mode II, and (iii) CZ–B2 failing in mixed-mode. Figures 2a and c show that increasing $T_{\mathrm{II}}^{\mathrm{B}}$ promotes CZ–A failure in mode I and CZ–B2 failure in mixed-mode, but hinders CZ–B1 failure in mode II. Although a very high level of damage (over 0.99) was reached in the cohesive elements in most investigated cases, no element is totally failed at $\varepsilon^{\infty} = 2\%$, which means that the proposed approach simulates cohesive fracture rather than brittle fracture.

It can be observed that normalised stress distributions for all cases presented in Figure 2 decrease monotonically from a peak value $k$ at the crack plane until a minimum ($\bar{\sigma} < 1$), after which $\bar{\sigma}$ increases asymptotically to $\bar{\sigma} = 1$.

Figure 2 shows that normalised stress distributions can be characterised by two values: the stress concentration factor $k \stackrel{\text{def}}{=} \bar{\sigma}(x = 0)$, and the recovery length $l_{\mathrm{k}}$, which is defined as the smallest distance from the crack plane to the position where $\bar{\sigma}$ equals 1 (so that $\bar{\sigma}(x = l_{\mathrm{k}}) = 1$).

The effect of cohesive zone properties on $k$ and $l_{\mathrm{k}}$ is presented in Figure 3, and the effect of interleaf properties on $k$ and $l_{\mathrm{k}}$ is presented in Figure 4.

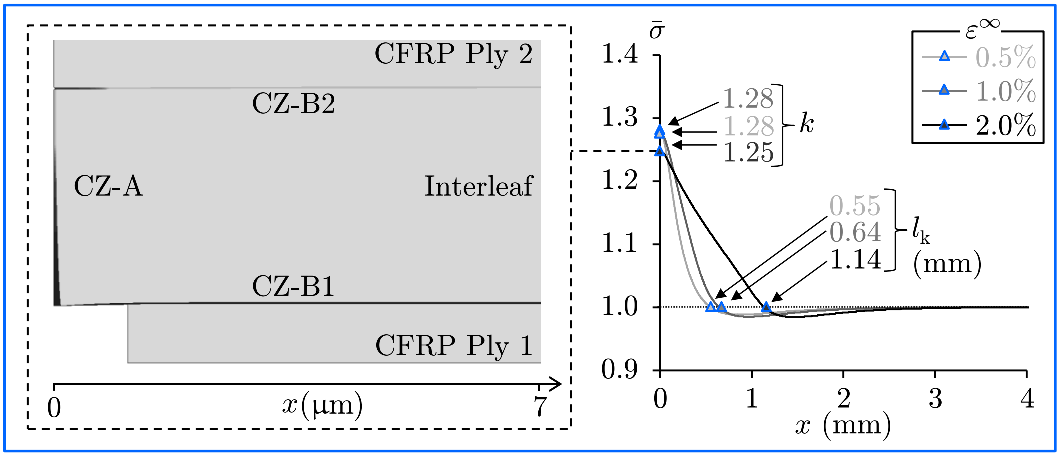


**(a)** $\frac{T_{II}^{B}}{T_{II}^{B,ref}} = 0.5$ ($T_{II}^{B} = 20$ MPa).

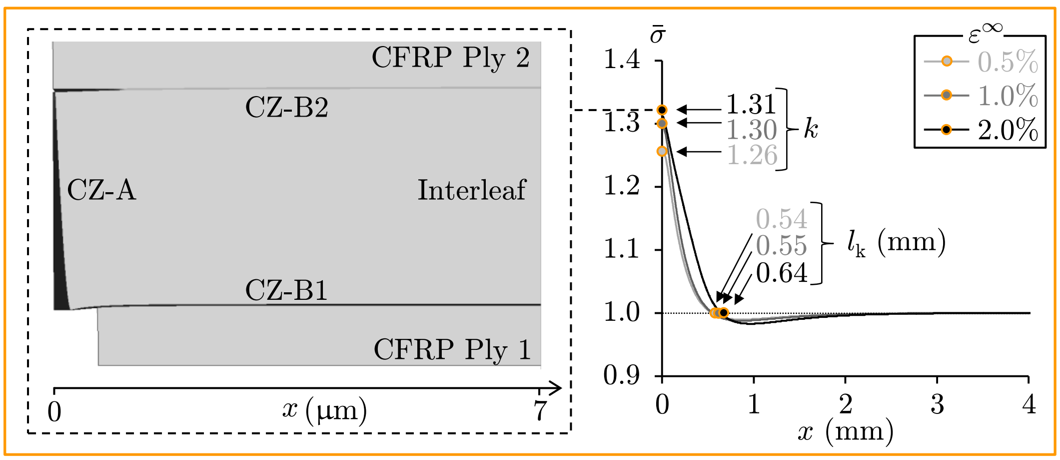


**(b)** $\frac{T_{II}^{B}}{T_{II}^{B,ref}} = 1.0$ ($T_{II}^{B} = 40$ MPa).

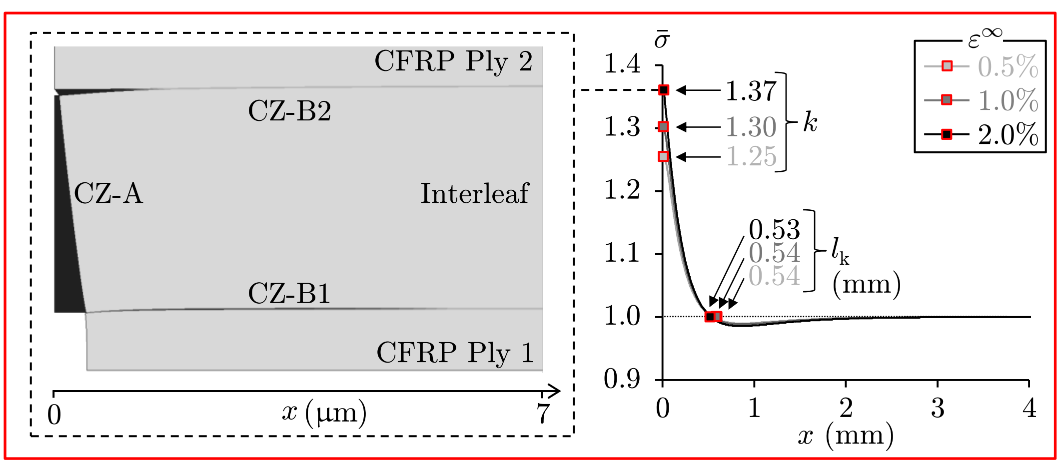


**(c)** $\frac{T_{II}^{B}}{T_{II}^{B,ref}} = 2.0$ ($T_{II}^{B} = 80$ MPa).

**Figure 2:** Stress and deformation fields in a PIC with a pre-fractured ply. Right: normalised stress distributions for different remote strains, where $k$ and $l_k$ are indicated by markers whose filled color (gradient of grey) identifies the level of remote strain. The markers' shape and color relate the applied CFRP/interleaf IFSS. This symbology remains identical hereafter. Left: deformed geometry at the vicinity of the initial crack for $\varepsilon^\infty = 2.0\%$ (the grey scale in the cohesive zones represents the damage variable). Subfigures (a) to (c) correspond to different CFRP/interleaf IFSS.

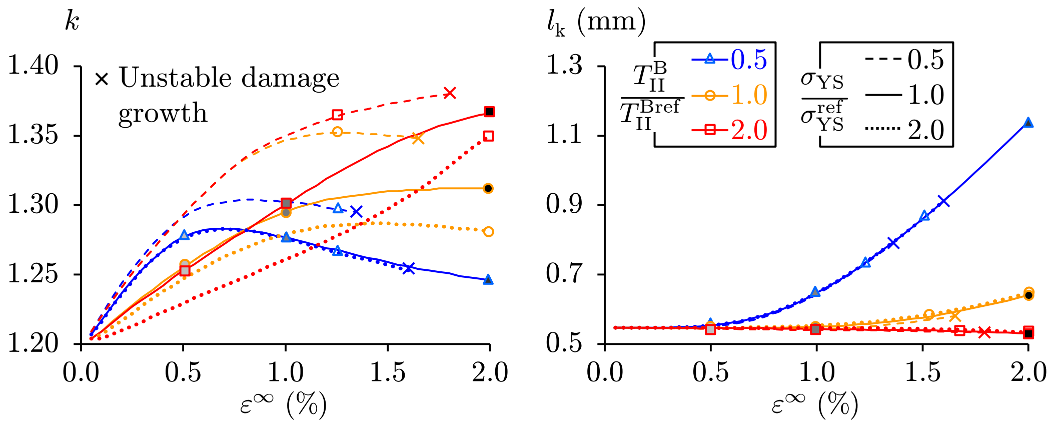


**(a)** Parametric study on the yield strength of the polymer (for different CFRP/interleaf IFSS).

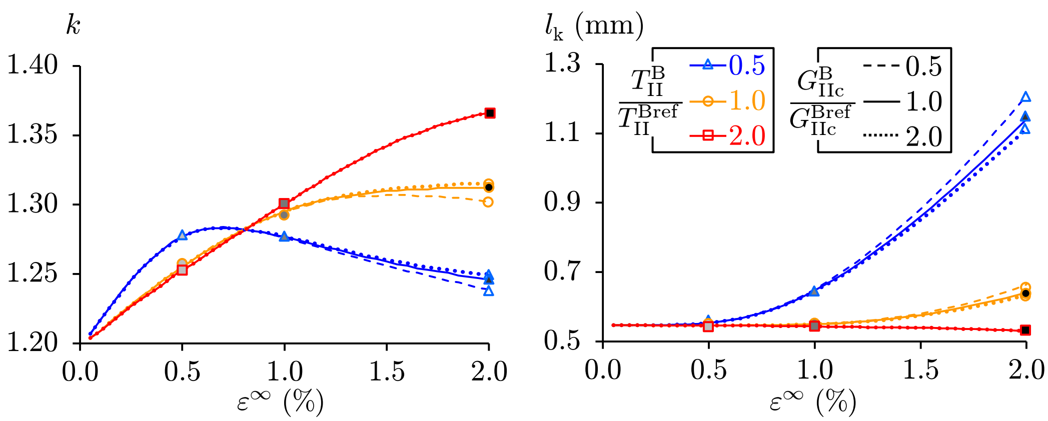


**(b)** Parametric study on the mode II delamination toughness of interfaces between the interleaf and neighbouring CFRP plies (for different CFRP/interleaf IFSS).

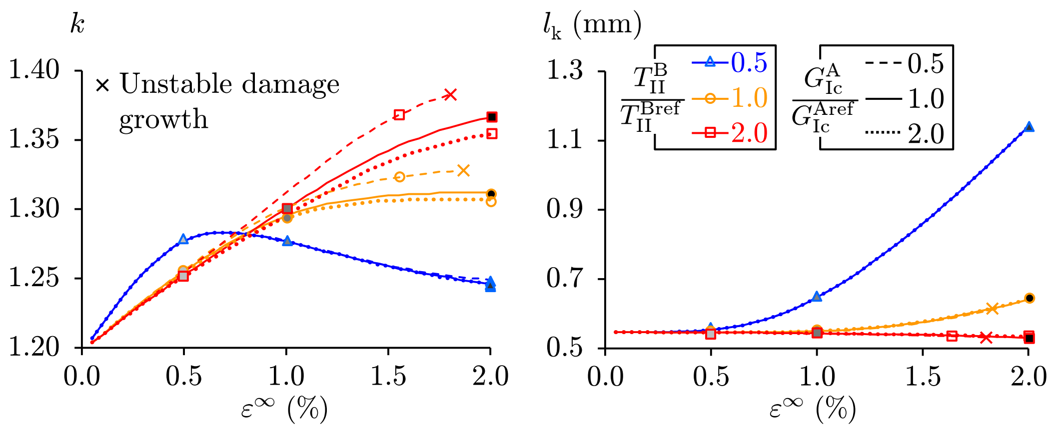


**(c)** Parametric study on the mode I opening toughness of the polymer (for different CFRP/interleaf IFSS).

**Figure 3:** Effect of the three parameters of the cohesive laws on the stress concentration factor ($k$, left) and the recovery length ($l_k$, right) distributions, for different CFRP/interleaf IFSS. For all graphs, solid lines are identical, and the notation was introduced in Figure 2.

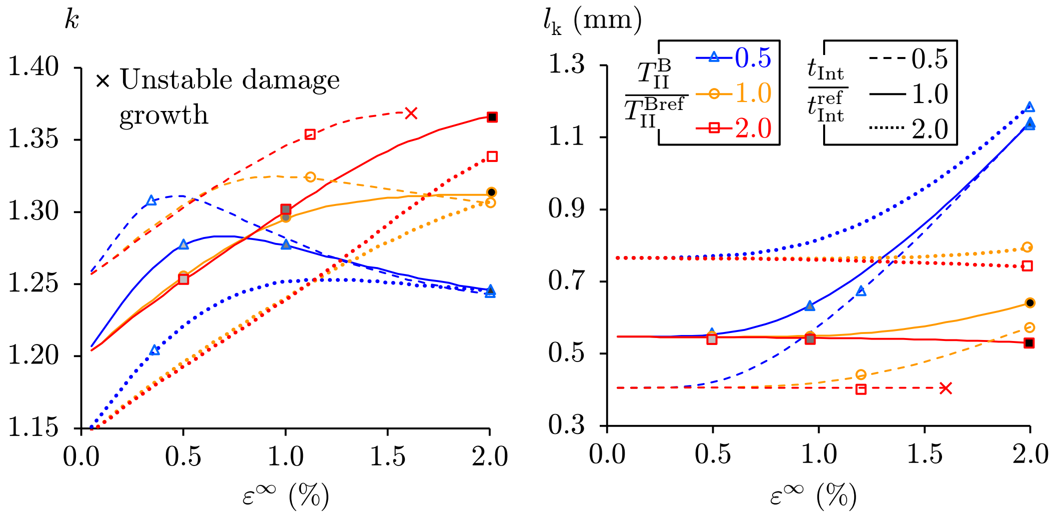


**(a)** Parametric study on the thickness of the polymer (for different CFRP/interleaf IFSS).

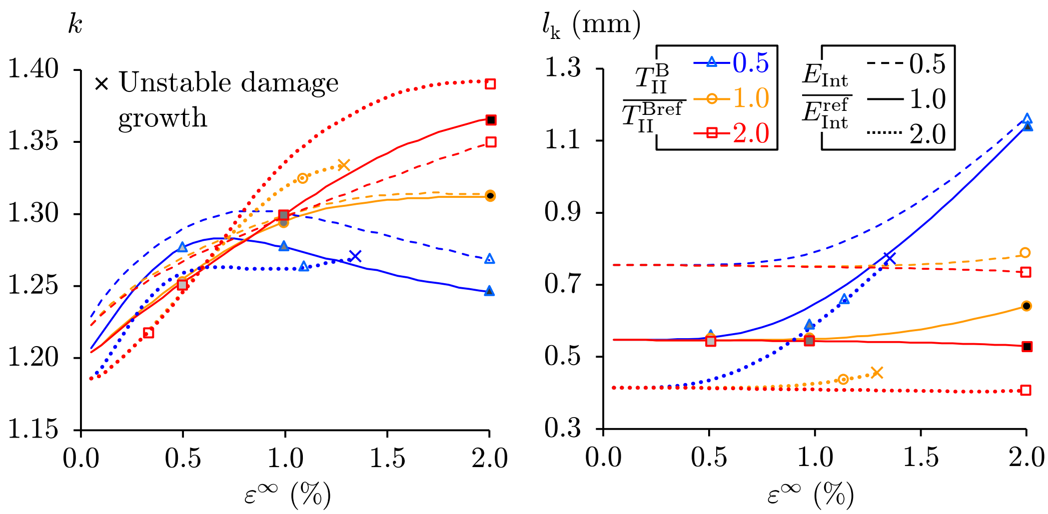


**(b)** Parametric study on the Young's modulus of the polymer (for different CFRP/interleaf IFSS).

**Figure 4:** Effect of interleaf thickness and Young's modulus on the stress concentration factor ($k$, graphs on the left) and the recovery length ($l_k$, right) distributions, for different CFRP/interleaf IFSS. For all graphs, solid lines are identical, and the notation was introduced in Figure 2.

### 3.2. Discussion of the analysis of failure processes

The results presented in Section 3.1 revealed the following:

- three different CZ damage processes were identified, corresponding to different damage mechanisms triggered by failure of CFRP Ply 1:
  - (i) CZ–A failing in mode I, corresponding to yielding/cracking of the interleaf under tension (see Figure 2c),

(ii) CZ–B1 failing in mode II, corresponding to interlaminar damage/delamination between the broken CFRP ply and the interleaf (see Figure 2a),

(iii) CZ–B2 failing in mixed-mode, corresponding to interlaminar damage/delamination and opening between the interleaf and the closest CFRP ply to the broken one (see Figure 2c).

- Mode II interlaminar damage between the broken CFRP ply and the interleaf is promoted by a low CFRP/interleaf IFSS (and by a high yield strength of the polymer). Reducing this IFSS, the stress concentration factor increases for low remote strains until significant interface damage has occurred (see $k$ increasing from $T_{\mathrm{II}}^{\mathrm{B}}/T_{\mathrm{II}}^{\mathrm{B,ref}} = 2.0$ to $T_{\mathrm{II}}^{\mathrm{B}}/T_{\mathrm{II}}^{\mathrm{B,ref}} = 0.5$ in Figure 3 for $\varepsilon^{\infty} < 0.5\%$). After this, and as the remote strain increases, the stress concentration factor decreases and the recovery length increases substantially due to delamination between the broken CFRP ply and the interleaf (see $k$ decreasing and $l_{\mathrm{k}}$ increasing for $T_{\mathrm{II}}^{\mathrm{B}}/T_{\mathrm{II}}^{\mathrm{B,ref}} = 0.5$ in Figure 3). As long as delamination governs the interlaminar damage process, the effect of other CZs' parameters on stress distributions are not significant (see blue curves in Figure 3, all dominated by delamination and therefore nearly coincident).

- Yielding/cracking of the interleaf is promoted by a strong CFRP/interleaf interface and a low yield strength of the interleaf polymer (*i.e.* the condition which inhibits damage at the CFRP/interleaf interface). Interleaf yielding/cracking increases the stress concentration factor without significant influence on the recovery length for large remote strains (see $k$ increasing and $l_{\mathrm{k}}$ decreasing slightly for $T_{\mathrm{II}}^{\mathrm{B}}/T_{\mathrm{II}}^{\mathrm{B,ref}} = 2.0$ in Figure 3 for $\varepsilon^{\infty} > 0.5\%$). A low mode I toughness of the polymer increases the effect of yielding/cracking of the interleaf on the stress concentration factor (Figure 3c).

- Mixed-mode damage of the interface between the interleaf and the closest CFRP ply to the broken one (see Figure 2) is promoted when yielding/cracking of the interleaf is promoted, hence by a strong CFRP/interleaf interface and a low yield strength of the interleaf polymer. However, for all cases studied, the process zone at the interface between the interleaf and the closest CFRP ply to the broken one was very short compared to the other ones, and had an insignificant effect on the stress distribution profile.

- The stress concentration factor decreases and the recovery length increases for thicker interleaves (see Figure 4a). Increasing the Young's modulus of the interleaf reduces the recovery length (see Figure 4a) and the stress concentration factor for low applied strain (*i.e.* low level of damage in CZs for $\varepsilon^{\infty} < 0.5\%$), but accentuates considerably the effect of yielding/cracking of the interleaf for high applied strain (see $k$ increasing significantly for $E_{\mathrm{Int}}/E_{\mathrm{Int}}^{\mathrm{ref}} = 2.0$ in Figure 4b for $\varepsilon^{\infty} > 0.5\%$). The influence of the CFRP/interleaf IFSS on the stress concentration factor and the recovery length is unaffected by changes in the thickness or the Young's modulus of the polymer.

These trends show that, in a PIC with one fractured ply, damage can be guided towards delamination or interleaf yielding/cracking, inducing differences in load transfer mechanisms, stress concentrations and recovery lengths. The parametric study shows that, at a remote strain of 1.5–2.0% (typical failure strain of UD composites), delamination between a fractured CFRP ply and an interleaf leads to low stress concentrations and to a large recovery length. Conversely, when the crack in a CFRP ply propagates transversely across the thickness of the interleaf, stress concentrations in the neighbouring CFRP ply are high and the recovery length is small. These different damage modes will therefore influence how likely the neighbouring CFRP plies are to fail unstably. This will be addressed in the next section.

## 4. Probability of catastrophic failure propagation in a PIC

### 4.1. Definition of stable and unstable failure

Figure 5 shows idealised stress distributions for two neighbouring CFRP plies in a PIC specimen of length $l_{\mathrm{s}}$ with $n$ plies. Figure 5a considers that CFRP Ply 1 is broken at $x = 0$, and the stress fields are piecewise linear approximations considering $k$ and $l_{\mathrm{k}}$ defined in Section 3 (only the right half of the stress distributions and only one of the two neighbouring plies are illustrated in Figure 5a due to double symmetry). In Figure 5b, a subsequent failure is considered in CFRP Ply 2 at $x = 2 \cdot l_{\mathrm{k}}$, which leads to similar stress concentrations as in CFRP Ply 1. Figure 5b shows that the stress fields due to each failure will interact if the two breaks are at a distance smaller than $2 \cdot l_{\mathrm{k}}$. Consequently, it is hereafter considered that a translaminar ply crack will propagate through-the-thickness of the PIC if one of the two neighbouring CFRP plies of the broken one fails within the control length, $l_{\mathrm{c}}$, centred at the first ply fracture, and defined as

$$l_{\mathrm{c}} = 4 \cdot l_{\mathrm{k}} \; . \tag{2}$$

Note that, since $l_{\mathrm{k}}$ depends on $\varepsilon^{\infty}$, so does $l_{\mathrm{c}}$.

In this work, failure of the PIC is classified as unstable if failure (at a given applied remote strain $\varepsilon^{\infty}$) of the weakest CFRP ply in the specimen (assumed to be CFRP ply 1) leads to failure of one of its two neighbouring CFRP plies (CFRP Ply 2) at the same strain level, within the control length. Conversely, failure is classified as stable if failure of the weakest CFRP ply does not lead to failure of one of its two neighbouring CFRP plies at the same strain within the control length. The probability of failure of the PIC being unstable is therefore

$$Pr^{\mathrm{unst}} = \int_{\varepsilon^{\infty}=0}^{\infty} F_{\mathrm{c}}^{(2)}(\varepsilon^{\infty}) \cdot \mathrm{d}F_{\mathrm{s}}^{(1)}(\varepsilon^{\infty}), \tag{3}$$

where $F_{\mathrm{s}}^{(1)}(\varepsilon^{\infty})$ is the cumulative failure probability for CFRP Ply 1 over the specimen length

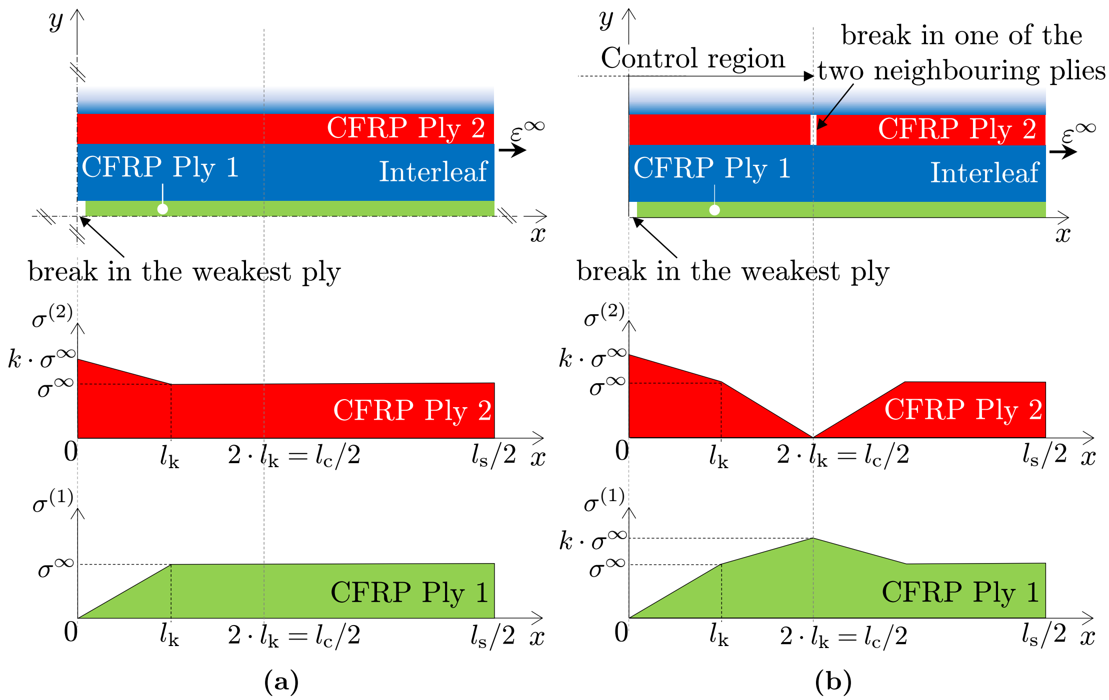


**Figure 5:** Simplified representations of stress distribution in CFRP plies 1 and 2 for two different configurations: (a) when CFRP Ply 1 fails and CFRP Ply 2 survives, and (b) when CFRP Ply 1 fails and CFRP Ply 2 fails at $x = l_c/2$.

$l_s$ and under an uniform remote strain $\varepsilon^\infty$, and $F_c^{(2)}(\varepsilon^\infty)$ is the cumulative failure probability of the two CFRP Ply 2 (the one represented in Figure 5 and the one in the symmetrical position below the $x$–axis) over the control region and under stress concentrations (as illustrated in a).

### 4.2. Calculation of the cumulative failure probabilities for CFRP Ply 1 and 2

Let $F_p\big(\sigma(\varepsilon^\infty)\big)$ be the cumulative failure probability of a CFRP ply with a reference length $l_p$ and under an uniform stress $\sigma(\varepsilon^\infty)$ induced by a remote strain $\varepsilon^\infty$. The corresponding survival probability is

$$S_p\big(\sigma(\varepsilon^\infty)\big) = 1 - F_p\big(\sigma(\varepsilon^\infty)\big). \tag{4}$$

Consider a PIC specimen with $n$ CFRP plies and a length $l_s$. Assuming that CFRP Ply 1 is the weakest out of $n$, then its cumulative failure probability distribution is

$$F_s^{(1)}(\varepsilon^\infty) = 1 - \left[S_s(\varepsilon^\infty)\right]^n, \tag{5}$$

where, according to the weakest link theory [26], $S_s(\varepsilon^\infty)$ is related to $S_p\big(\sigma(\varepsilon^\infty)\big)$ by

$$\ln\left[S_s(\varepsilon^\infty)\right] = \frac{l_s}{l_p} \cdot \ln\left[S_p\big(\sigma(\varepsilon^\infty)\big)\right]. \tag{6}$$

Consider that CFRP Ply 1 is now broken (Figure 5a). The survival probability of the neighbouring plies of CFRP Ply 1 in the control region (*i.e.* four segments of CFRP Ply 2 of length $l_\mathrm{c}/2$ and stress distributions as illustrated in Figure 5a), $S_\mathrm{c}^{(2)}(\varepsilon^\infty)$, can be calculated from

$$\ln\left[S_\mathrm{c}^{(2)}(\varepsilon^\infty)\right] = \frac{4}{l_\mathrm{p}}\int_0^{l_\mathrm{c}/2} \ln\left[S_\mathrm{p}\big(\sigma^{(2)}(x,\varepsilon^\infty)\big)\right]\mathrm{d}x, \tag{7}$$

where $\sigma^{(2)}(\varepsilon^\infty)$ (illustrated in Figure 5a) is the stress distribution in CFRP Ply 2. The factor 4 comes because the integration is only carried over $l_\mathrm{c}/2$ for one of the two neighbouring plies. The cumulative failure probability of the two neighbouring plies of the broken one is finally

$$F_\mathrm{c}^{(2)}(\varepsilon^\infty) = 1 - S_\mathrm{c}^{(2)}(\varepsilon^\infty). \tag{8}$$

Equations 5 and 8 are used in Equation 3 to calculate the probability of unstable failure.

### 4.3. Parametric studies on the probability of unstable failure

The probability of unstable failure will be calculated for the PIC analysed in Section 3, with a length $l_\mathrm{s} = 100$ mm. This requires the cumulative failure probability distributions (i) of the weakest ply out of n=7 ($F_\mathrm{s}^{(1)}$), and (ii) of CFRP Ply 2 under stress concentrations and within the control region ($F_\mathrm{c}^{(2)}$). As described in Section 4.2, these two distributions require:

(a) the stress distribution in CFRP Ply 2, $\sigma^{(2)}(\varepsilon^\infty)$ (needed in Equation 7). This was calculated by the FEM in Section 3.

(b) the strength distribution for a CFRP ply, $F_\mathrm{p}\big(\sigma(\varepsilon^\infty)\big)$ (needed in Equation 4). This was calculated using a previously developed hierarchical strength model for UD CFRPs [4]. The model calculates the strength distribution of a UD ply with a given number of fibres and a given length, from the strength of individual fibres (modelled by a Weibull distribution) and the matrix behaviour (represented through a perfectly plastic shear-lag model at the fibre level), with properties given in Table 3.

As the strength distribution for a UD composite depends on the number of fibres it contains, the cumulative failure probabilities $F_\mathrm{s}^{(1)}$ and $F_\mathrm{c}^{(2)}$ will be influenced by the width of the PIC specimen (which did not need to be defined for the FE analysis). Consequently, a range of specimen widths between 27 μm (square ply cross section, 8 fibres per ply) and 14 mm (4096 fibres per ply) are considered.

In order to study the influence of a broad range of possible geometries and material properties on the probability of unstable failure of a PIC, six cases were selected from the parametric study presented in Section 3, as detailed in Table 4.

**Table 3:** Properties of TR30 fibres and K50 matrix used to calculate the cumulative strength distribution $F_\mathrm{p}\big(\sigma(\varepsilon^\infty)\big)$ using the model by Pimenta and Pinho [4]. $\sigma_0^\mathrm{f}$ and $m$ are respectively the shape and scale parameters of the Weibull distribution, calculated from the average strength of fibres $X^\mathrm{f}$, measured at $l_\mathrm{p}$, and the coefficient of variation of the strength distribution $\mathrm{CoV}_X^\mathrm{f}$.

| **TR30 fibres** | | | | | | | **K50 matrix** |
|---|---|---|---|---|---|---|---|
| Young's modulus | Strength distribution | | | | | Diameter | Shear lag strength |
| $E^\mathrm{f}$ (GPa) | $X^\mathrm{f}$ (GPa) | $\mathrm{CoV}_X^\mathrm{f}$ (%) | $l_\mathrm{p}$ (mm) | $\sigma_0^\mathrm{f}$ (GPa) | $m$ (–) | $\phi^\mathrm{f}$ (μm) | $T_\mathrm{SL}$ (MPa) |
| $235^{(\star)}$ | 4.28 [41] | 18.5 [41] | 25 [41] | 7.67 | 6.31 | 7 [41] | $87.7^{(\dagger)}$ |

$^{(\star)}$ Provided by the manufacturer
$^{(\dagger)}$ Measured on 16 ply UD laminates

**Table 4:** Specifications of cases used to study the influence of geometrical and material properties on the probability of unstable failure of a PIC. For all cases, $\sigma_\mathrm{YS}$, $G_\mathrm{IIc}^\mathrm{B}$ and $G_\mathrm{Ic}^\mathrm{A}$ are equal to their respective reference values shown in Table 2. The resulting $k$ and $l_\mathrm{k}$ are qualitatively evaluated in comparison to those in the reference distribution, following this symbology: ref (reference distribution), + (higher), − (lower).

| **Case** | $\frac{T_\mathrm{II}^\mathrm{B}}{T_\mathrm{II}^\mathrm{B,ref}}$ | $\frac{E_\mathrm{Int}}{E_\mathrm{Int}^\mathrm{ref}}$ | $\frac{t_\mathrm{Int}}{t_\mathrm{Int}^\mathrm{ref}}$ | $k$ | $l_\mathrm{k}$ | Distributions shown in |
|---|---|---|---|---|---|---|
| 1 | 2 | 2 | 1 | ++ | −− | Figure 4b (dotted red curve) |
| 2 | 2 | 1 | 1 | + | − | Figure 3 (solid red curve) |
| 3 | 1 | 1 | 1 | ref | ref | Figure 3 (solid orange curve) |
| 4 | 0.5 | 0.5 | 1 | − | ++ | Figure 4b (dashed blue curve) |
| 5 | 0.5 | 1 | 1 | − | + | Figure 3 (solid blue curve) |
| 6 | 0.5 | 1 | 0.5 | −− | + | Figure 4a (dashed blue curve) |

### 4.4. Results for the probability of unstable failure of a PIC

Predicted probabilities of unstable failure (Equation 3) are shown in Figure 6. Figure 7 shows two sets of predicted cumulative failure probabilities (Equations 5 and 8), one related to the narrow specimen (27 μm width, 8 fibres, dashed lines) and the other one to the wide specimen (14 mm, 4096 fibres, solid lines).

Figure 6 shows that, regardless of the geometrical and material properties, the probability of unstable failure decreases significantly while decreasing the width of the specimen. A decrease while moving from case 1 to case 6 is also observed (where case 1 promotes yielding/cracking of the interleaf and case 6 promotes delamination between the broken CFRP ply and the interleaf), with a more significant effect for a wide specimen (decrease of 30% from case 1 to case 6), than for a narrow specimen (decrease of 6.2% from case 1 to case 6).

By increasing the width of the specimen (and consequently the number of fibres it contains), the strength variability of each ply decreases [4], which has a strong influence on predicted strength distributions and, consequently, on the probability of unstable failure. This point is illustrated in Figure 7, which shows that, for a wide specimen (*i.e.* with low strength variability), predicted cumulative failure probabilities of the neighbouring plies of CFRP Ply 1 over the control region are mostly higher than the cumulative failure probability of CFRP Ply 1 over the entire length of the specimen, leading to a high probability of unstable failure. For a narrow specimen (*i.e.* with high strength variability), all predicted cumulative failure probabilities of the neighbouring plies of CFRP Ply 1 over the control region are lower than the cumulative failure probability of CFRP Ply 1 over the entire length of the specimen, leading to a low probability of unstable failure.

Regardless the specimen width, it can also be observed in Figure 7 that the cumulative failure probability of CFRP Ply 2 over the control region, under stress concentrations, decreases while going from case 1 (dominated by interleaf damage) to case 6 (dominated by delamination), explaining the trends shown on Figure 6.

### 4.5. Discussion on the potential of interleaving to delay catastrophic failure in UD composites

It must be noted that although the combined FE/statistical approach presents several limitations mentioned in Section 2 (residual thermal stresses and chemical interactions between the interleaves and the CFRP plies were neglected, stresses in CFRP Ply 2 have been homogenised) which could lead to different quantitative predictions, they should not affect the qualitative trends discussed in this section. Regarding the probability of unstable failure

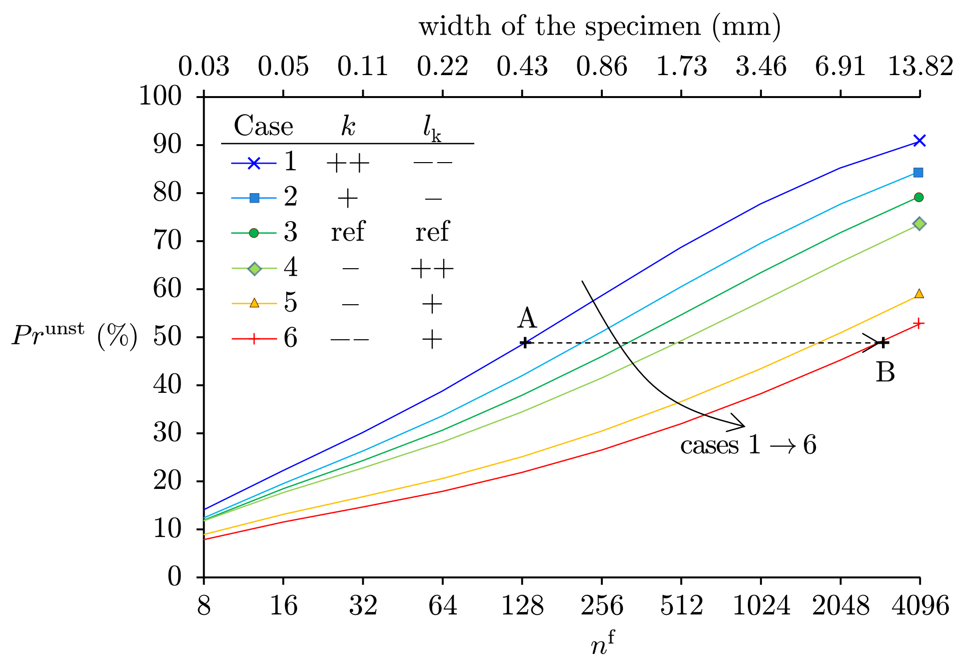


**Figure 6:** Probabilities of unstable failure predicted by the model for the six cases identified in Table 4, for different number of fibres in CFRP plies. The resulting $k$ and $l_{\mathrm{k}}$ are indicated for each case following the symbology given in Table 4. Points A and B have the same probability of unstable failure, but correspond to different PIC configurations and different specimen widths.

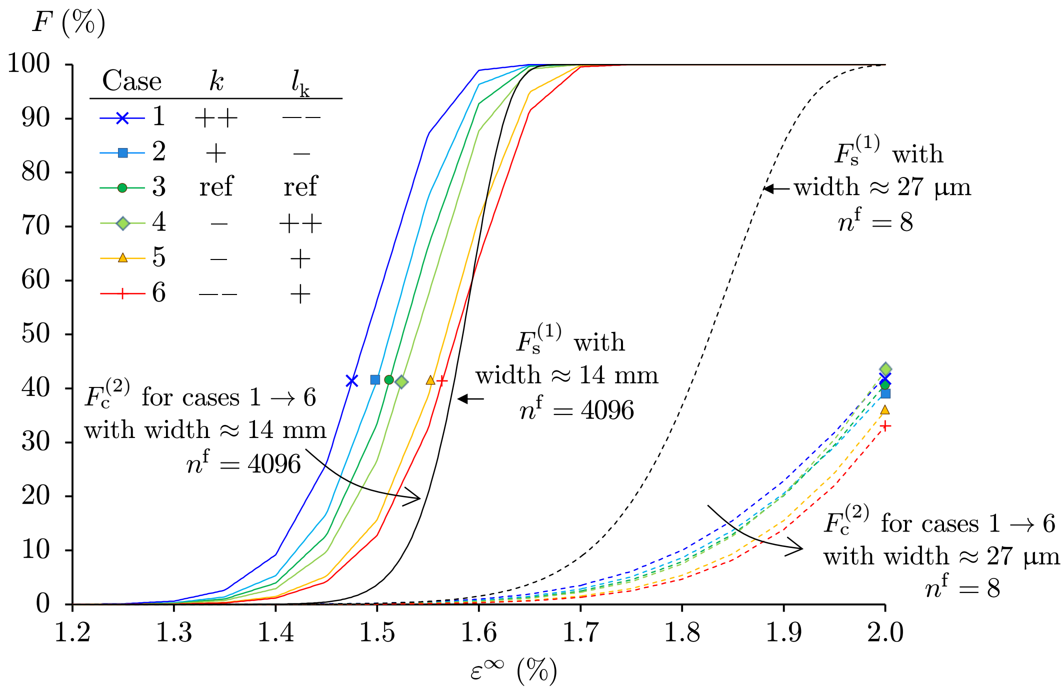


**Figure 7:** Overview of cumulative failure probabilities predicted by the model for the six cases identified in Table 4, for two different numbers of fibres in the CFRP plies: one with 4100 fibres (solid lines), and another one with 16 fibres (dashed lines). The resulting $k$ and $l_\mathrm{k}$ are indicated for each case following the symbology given in Table 4.

of PICs, Figures 6 and 7 show that:

(O1) the crucial feature required to avoid PIC catastrophic (unstable) failure is to increase considerably the strength variability of the CFRP plies.

(O2) reducing $k$ and $l_\mathrm{k}$ decreases the probability of unstable failure in PIC specimens, but the influence of $k$ is more significant. To reduce $k$, as explained in Section 3.2, yielding/cracking of the interleaf must be avoided, and delamination (or interlaminar damage) between the broken CFRP ply and the interleaf must be promoted. However, a full delamination across the entire specimen should be avoided to allow for stress recovery in the fractured ply.

Observations (O1) and (O2) show that interleaving can decrease the probability of unstable failure propagating in a composite laminate under tensile load from a transverse crack in a CFRP ply of any size. However, the true potential of interleaving for delaying catastrophic failure propagation in a UD composite lies with configurations with intermediate number of fibres per ply. Experimental observations [2, 3] performed on UD composites under longitudinal tension have shown that composites fail as soon as a cluster of broken fibres reaches a critical size. The current work shows that with an optimised PIC, it is possible to increase significantly the size of the critical cluster of broken fibres that the composite can withstand by controlling the interlaminar damage. For instance, the configuration B shown in Figure 6 (PIC of type 6, dominated by delamination) with 3100 fibres has the same probability of unstable failure (50%) as the configuration A shown in Figure 6 (PIC of type 1, dominated by interleaf damage) with 128 fibres.

The potential of interleaving remains to be experimentally investigated. For that, the parametric study can provide guidance for manufacturing PIC specimens which could exhibit a high probability of stable failure:

- in order to increase the strength variability in CFRP plies as much as possible, a possibility is to drastically decrease the number of fibres in each ply, by using for instance thin-ply prepregs (their thickness can now be down to 22 µm [19]), or composite micro fibre–bundles of 8–32 fibres.
- in order to decrease stress concentrations in CFRP plies neighbouring a ply break, delamination at the CFRP ply/interleaf interface must be promoted, while the delaminated length must be limited to allow for multi-fragmentation of the broken CFRP ply. Results given in Figure 6 show that the best way to achieve that is to manufacture a PIC specimen (configuration 6) with a low CFRP/interleaf IFSS and a thin interleaf.

## 5. Conclusions

A combined FEM-statistical approach was proposed to investigate the potential of interleaving to delay catastrophic failure in UD composite under tensile load. The tensile response of damaged PICs was studied, stress concentrations in the two closest neighbouring plies of a failed ply were predicted, and the resulting failure mechanisms were analysed.

The present approach demonstrated that the probability of unstable failure of PICs can be reduced by two different ways. The first one is to provide sufficient strength variability for the CFRP plies, for instance by decreasing the number of fibres they contain. The other way is to decrease as much as possible stress concentrations around ply breaks, by promoting a limited amount of delamination or damage between interleaves and CFRP plies in the vicinity of a CFRP translaminar ply crack. In this case, the critical cluster size of broken fibres can increase significantly (by two orders of magnitude) with optimised interlaminar properties.

Interleaving has been shown to have the potential for delaying catastrophic failure in a UD composite. It permits a larger critical cluster of broken fibres, which enables a more stable propagation of damage across the thickness of PIC specimens with optimised geometrical and mechanical properties. This potential remains to be experimentally investigated.

## Appendix A. Estimation of cohesive law parameters for the model described in Section 2

### A.1. Known parameters

Three parameters were used to estimate the ones required for the two bilinear traction-separation laws defined in the presented FEM (see Section 2.2.2): (i) the yield stress of the polymer ($\sigma_{\mathrm{YS}}$), (ii) the CFRP/interleaf Interfacial Shear Strength (IFSS, $T_{\mathrm{II}}^{\mathrm{B}}$), and (iii) the mode II delamination toughness ($G_{\mathrm{IIc}}^{\mathrm{B}}$) between the interleaf and the CFRP.

### A.2. Penalty stiffnesses $K_{\mathrm{I}}$ and $K_{\mathrm{II}}$

The following $K_{\mathrm{I}}$ and $K_{\mathrm{II}}$ were used:

$$K_{\mathrm{I}} = 2 \cdot 10^6 \ \mathrm{N/mm^3}, \text{ and } K_{\mathrm{II}} = 1 \cdot 10^6 \ \mathrm{N/mm^3}. \tag{A.1}$$

These relations ensure high enough values for reasonable penalty stiffness while avoiding numerical convergence issues [27].

### A.3. Traction $T_{\mathrm{I}}^{\mathrm{A}}$

$T_{\mathrm{I}}^{\mathrm{A}}$ was estimated by applying Hill's criterion [28], after assuming $T_{\mathrm{I}}^{\mathrm{A}}$ to be equal to the maximum net section stress for single edge notched tensile, which leads to the simple relation

$$T_{\mathrm{I}}^{\mathrm{A}} = \sigma_{\mathrm{YS}}. \tag{A.2}$$

### A.4. Fracture toughness $G_{\mathrm{Ic}}^{\mathrm{A}}$

Fracture toughness values in mode I can be found in literature for several different polymers and composite materials, but many studies showed that this parameter depends on the interlaminar thickness when the latter becomes smaller than the radius of the plastic zone at the crack tip [11, 21, 29–31]. Some methods were suggested to measure this property for ductile polymers with very small ligament length [32, 33], but the determination of consistent fracture toughness values for polymer film as thin as the ones considered in this study (25–100 µm) is still an unsolved issue [34–36].

In the absence of reliable experimental values, a reference fracture toughness $G_{\mathrm{Ic}}^{\mathrm{A,ref}}$ was estimated based on the transitional polymer fracture toughness when the equivalent plastic zone radius is approximatively equal to the interleaf thickness [37]. This is calculated from Irwin's first-order estimation of the related plastic zone size at the crack tip of an infinite plate of an elasto-plastic material subjected to uniform tension [38]:

$$r_{\mathrm{Y}} = \frac{1}{2\pi} \left( \frac{K_{\mathrm{I}}}{\sigma_{\mathrm{YS}}^{\mathrm{ref}}} \right)^2, \tag{A.3}$$

where $K_{\mathrm{I}} = \sqrt{G \cdot E^{\mathrm{ref}}}$ is the stress intensity factor, $G$ is the energy release rate, $E^{\mathrm{ref}}$ and $\sigma_{\mathrm{YS}}^{\mathrm{ref}}$ are respectively the Young's modulus and the yield stress of the material, and $r_{\mathrm{Y}}$ is the plastic zone radius. For the polymer interleaf, assuming $G = G_{\mathrm{Ic}}^{\mathrm{A,ref}}$ when $r_{\mathrm{Y}} = t_{\mathrm{Int}}$ leads to

$$G_{\mathrm{Ic}}^{\mathrm{A,ref}} = \frac{2\pi \cdot t_{\mathrm{Int}}}{E^{\mathrm{ref}}} \left(\sigma_{\mathrm{YS}}^{\mathrm{ref}}\right)^2 . \tag{A.4}$$

This estimation is consistent with the approach in Section A.3.

### A.5. Fracture toughnesses $G_{\mathrm{IIc}}^{\mathrm{A}}$ and $G_{\mathrm{Ic}}^{\mathrm{B}}$

$G_{\mathrm{IIc}}^{\mathrm{A}}$ and $G_{\mathrm{Ic}}^{\mathrm{B}}$ were calculated from $G_{\mathrm{Ic}}^{\mathrm{A}}$ and $G_{\mathrm{IIc}}^{\mathrm{B}}$ values by applying a fixed toughness ratio

$$\frac{G_{\mathrm{Ic}}}{G_{\mathrm{IIc}}} = 0.5 \tag{A.5}$$

for both cohesive laws. This ratio is in good agreement with experimental studies performed on composites laminates [39], as well as on thin polymer films [35].

### A.6. Tractions $T_{\mathrm{II}}^{\mathrm{A}}$ and $T_{\mathrm{I}}^{\mathrm{B}}$

$T_{\mathrm{II}}^{\mathrm{A}}$ and $T_{\mathrm{I}}^{\mathrm{B}}$ were estimated using the following relations [40]:

$$T_{\mathrm{II}}^{\mathrm{A}} = T_{\mathrm{I}}^{\mathrm{A}} \cdot \sqrt{\frac{G_{\mathrm{IIc}}^{\mathrm{A}}}{G_{\mathrm{Ic}}^{\mathrm{A}}}} \text{ and} \tag{A.6}$$

$$T_{\mathrm{I}}^{\mathrm{B}} = T_{\mathrm{II}}^{\mathrm{B}} \cdot \sqrt{\frac{G_{\mathrm{Ic}}^{\mathrm{B}}}{G_{\mathrm{IIc}}^{\mathrm{B}}}} . \tag{A.7}$$

### A.7. Conclusion on the estimation of cohesive law parameters

The assumptions presented in Appendix A lead to a reduction of unknown parameters required for setting up the two cohesive laws, from twelve to only three: $\sigma_{\mathrm{YS}}$, $T_{\mathrm{II}}^{\mathrm{B}}$ and $G_{\mathrm{IIc}}^{\mathrm{B}}$.

## Acknowledgements

This work was funded under the EPSRC Programme Grant EP/I02946X/1 on High Performance Ductile Composite Technology, in collaboration with the University of Bristol. The authors gratefully acknowledge Jonathan Fuller (University of Bristol) for the measurements he performed on Skyflex USN020A CFRP.

## References

[1] W. A. Curtin, *Stochastic Damage Evolution and Failure in Fiber-Reinforced Composites*, vol. 36, pp. 163–253. Elsevier, 1998.

[2] D. R.-B. Aroush, E. Maire, C. Gauthier, S. Youssef, P. Cloetens, and H. D. Wagner, "A study of fracture of unidirectional composites using in situ high-resolution synchrotron X-ray microtomography," *Composites Science and Technology*, vol. 66, no. 10, pp. 1348–1353, 2006.

[3] A. E. Scott, M. Mavrogordato, P. Wright, I. Sinclair, and S. M. Spearing, "In situ fibre fracture measurement in carbonepoxy laminates using high resolution computed tomography," *Composites Science and Technology*, vol. 71, no. 12, pp. 1471–1477, 2011.

[4] S. Pimenta and S. T. Pinho, "Hierarchical scaling law for the strength of composite fibre bundles," *Journal of the Mechanics and Physics of Solids*, vol. 61, no. 6, pp. 1337–1356, 2013.

[5] A. Thionnet, H. Y. Chou, and A. Bunsell, "Fibre break processes in unidirectional composites," *Composites Part A: Applied Science and Manufacturing*, vol. 65, pp. 148–160, 2014.

[6] W. S. Chan, "Delamination arrester - an adhesive inner layer in laminated composites," in *Composite Materials: Fatigue and Fracture: a Symposium Sponsored by ASTM Comittee D-30 on High Modulus Fibers and Their Composites*, vol. 907, pp. 176–196, ASTM International, 1986.

[7] F. Gao, G. Jiao, Z. Lu, and R. Ning, "Mode II delamination and damage resistance of carbon/epoxy composite laminates interleaved with thermoplastic particles," *Journal of Composite Materials*, vol. 41, no. 1, pp. 111–123, 2007.

[8] J. M. Scott and D. C. Phillips, "Carbon fibre composites with rubber toughened matrices," *Journal of Materials Science*, vol. 10, no. 4, pp. 551–562, 1975.

[9] S. F. Chen and B. Z. Jang, "Fracture behaviour of interleaved fiber-resin composites," *Composites Science and Technology*, vol. 41, no. 1, pp. 77–97, 1991.

[10] A. Duarte, I. Herszberg, and R. Paton, "Impact resistance and tolerance of interleaved tape laminates," *Composite Structures*, vol. 47, no. 14, pp. 753–758, 1999.

[11] S. Singh and I. K. Partridge, "Mixed-mode fracture in an interleaved carbon-fibre/epoxy composite," *Composites Science and Technology*, vol. 55, no. 4, pp. 319–327, 1995.

[12] M. Hojo, S. Matsuda, M. Tanaka, S. Ochiai, and A. Murakami, "Mode I delamination fatigue properties of interlayer-toughened CF/epoxy laminates," *Composites Science and Technology*, vol. 66, no. 5, pp. 665–675, 2006.

[13] S. Sihn, R. Y. Kim, K. Kawabe, and S. W. Tsai, "Experimental studies of thin-ply laminated composites," *Composites Science and Technology*, vol. 67, no. 6, pp. 996–1008, 2007.

[14] T. Yokozeki, Y. Aoki, and T. Ogasawara, "Experimental characterization of strength and damage resistance properties of thin-ply carbon fiber/toughened epoxy laminates," *Composite Structures*, vol. 82, no. 3, pp. 382–389, 2008.

[15] J. W. Hutchinson, "Mixed mode fracture mechanics of interfaces," *Metal and Ceramic interfaces*, pp. 295–306, 1990.

[16] B. D. Davidson and H. Hu, "Effect of interlayer modulus on fracture mode ratio for interleaved composite laminates," *Engineering Fracture Mechanics*, vol. 52, no. 2, pp. 243–253, 1995.

[17] C. Shet and N. Chandra, "Effect of the shape of T-$\delta$ cohesive zone curves on the fracture

response," *Mechanics of Advanced Materials and Structures*, vol. 11, no. 3, pp. 249–275, 2004.

[18] Dassault Systemes Simulia Corp., "ABAQUS user's manual," 2013.

[19] G. Czèl and M. R. Wisnom, "Demonstration of pseudo-ductility in high performance glass/epoxy composites by hybridisation with thin-ply carbon prepreg," *Composites Part A: Applied Science and Manufacturing*, vol. 52, pp. 23–30, 2013.

[20] L. Landro and M. Pegoraro, "Carbon fibre thermoplastic matrix adhesion," *Journal of Materials Science*, vol. 22, no. 6, pp. 1980–1986, 1987.

[21] N. Sela, O. Ishai, and L. Banks-Sills, "The effect of adhesive thickness on interlaminar fracture toughness of interleaved CFRP specimens," *Composites*, vol. 20, no. 3, pp. 257–264, 1989.

[22] O. Ishai, H. Rosenthal, N. Sela, and E. Drukker, "Effect of selective adhesive interleaving on interlaminar fracture toughness of graphite/epoxy composite laminates," *Composites*, vol. 19, no. 1, pp. 49–54, 1988.

[23] H. Ming-Yuan and J. W. Hutchinson, "Crack deflection at an interface between dissimilar elastic materials," *International Journal of Solids and Structures*, vol. 25, no. 9, pp. 1053–1067, 1989.

[24] H. Ming Yuan, A. G. Evans, and J. W. Hutchinson, "Crack deflection at an interface between dissimilar elastic materials: Role of residual stresses," *International Journal of Solids and Structures*, vol. 31, no. 24, pp. 3443–3455, 1994.

[25] Dassault Systemes Simulia Corp., "ABAQUS Scripting Reference Manual," 2014.

[26] W. Weibull, "A statistical distribution function of wide applicability," *Journal of applied mechanics*, pp. 293–297, 1951.

[27] A. Turon, C. G. Dávila, P. P. Camanho, and J. Costa, "An engineering solution for mesh size effects in the simulation of delamination using cohesive zone models," *Engineering Fracture Mechanics*, vol. 74, no. 10, pp. 1665–1682, 2007.

[28] R. Hill, "On discontinuous plastic states, with special reference to localized necking in thin sheets," *Journal of the Mechanics and Physics of Solids*, vol. 1, no. 1, pp. 19–30, 1952.

[29] A. Aksoy and L. A. Carlsson, "Crack tip yield zone estimates in mode II interlaminar fracture of interleaved composites," *Engineering Fracture Mechanics*, vol. 39, no. 3, pp. 525–534, 1991.

[30] F. Ozdil and L. A. Carlsson, "Plastic zone estimates in mode I interlaminar fracture of interleaved composites," *Engineering Fracture Mechanics*, vol. 41, no. 5, pp. 645–658, 1992.

[31] U. Zerbst, M. Heinimann, C. D. Donne, and D. Steglich, "Fracture and damage mechanics modelling of thin-walled structures – an overview," *Engineering Fracture Mechanics*, vol. 76, no. 1, pp. 5–43, 2009.

[32] K. B. Broberg, "Crack-growth criteria and non-linear fracture mechanics," *Journal of the Mechanics and Physics of Solids*, vol. 19, no. 6, pp. 407–418, 1971.

[33] Y.-W. Mai and B. Cotterell, "On the essential work of ductile fracture in polymers," *International Journal of Fracture*, vol. 32, no. 2, pp. 105–125, 1986.

[34] S. Hashemi, "Fracture toughness evaluation of ductile polymeric films," *Journal of Ma-*

*terials Science*, vol. 32, no. 6, pp. 1563–1573, 1997.

[35] T. Bárány, T. Czigány, and J. Karger-Kocsis, "Application of the essential work of fracture (EWF) concept for polymers, related blends and composites: A review," *Progress in Polymer Science*, vol. 35, no. 10, pp. 1257–1287, 2010.

[36] F. Tuba, L. Oláh, and P. Nagy, "On the valid ligament range of specimens for the essential work of fracture method: The inconsequence of stress criteria," *Engineering Fracture Mechanics*, vol. 99, pp. 349–355, 2013.

[37] L. Hunston D, "Composite interlaminar fracture: Effect of matrix fracture energy," *Composites technology review*, vol. 6, no. 4, pp. 176–180, 1984.

[38] G. R. Irwin, "Analysis of stresses and strains near the end of a crack traversing a plate.," *J. Appl. Physics*, vol. 24, p. 4, 1957.

[39] Q. Yang and B. Cox, "Cohesive models for damage evolution in laminated composites," *International Journal of Fracture*, vol. 133, no. 2, pp. 107–137, 2005.

[40] A. Turon, P. P. Camanho, J. Costa, and J. Renart, "Accurate simulation of delamination growth under mixed-mode loading using cohesive elements: Definition of interlaminar strengths and elastic stiffness," *Composite Structures*, vol. 92, no. 8, pp. 1857–1864, 2010.

[41] T. R. Pozegic, I. Hamerton, J. V. Anguita, W. Tang, P. Ballocchi, P. Jenkins, and S. R. P. Silva, "Low temperature growth of carbon nanotubes on carbon fibre to create a highly networked fuzzy fibre reinforced composite with superior electrical conductivity," *Carbon*, vol. 74, pp. 319–328, 2014.